Spontaneous emission in a subwavelength environment characterized by boundary integral equations

L. Rogobete
Nano-Optics Group, Laboratory of Physical Chemistry, Swiss Federal Institute of Technology (ETH), Zurich, Switzerland

C. Henkel*
Institute of Physics, University of Potsdam, Potsdam, Germany
(Received 1 July 2004; published 22 December 2004)

We discuss the impact of a dielectric nanoparticle on the fluorescence light from an emitter embedded in the particle. Numerical and analytical calculations predict a slower radiative decay compared to a bulk dielectric due to electrostatic screening. We assess the relevance of the nanoparticle shape and size and the position and orientation of the molecule. The numerical results are obtained from a rigorous solution of the Maxwell equations, formulated as boundary integral equations.

DOI: 10.1103/PhysRevA.70.063815 PACS number(s): 42.50.Nn, 42.25.Bs, 68.37.Uv

I. INTRODUCTION

The spontaneous emission rate of an excited atom or molecule is not an intrinsic property, but depends on the matter surrounding the emitter. This fact is now well appreciated after many years of research in the field of cavity quantum electrodynamics. More recently, the interaction of single emitters with their environment has opened the perspective of using them as sensitive probes with high spatial resolution, in particular in near-field scanning optical microscopy (SNOM) [1]. Indeed, their radiative properties (spontaneous emission rate, scattering cross section) are significantly changed at subwavelength distances from interfaces and nanostructures, due to the coupling to the electromagnetic near field. In this nanoscopic regime, cavity or standing-wave resonances are less relevant, and the light emission is dominated on the contrary by nonradiative or evanescent components of the field, as soon as these are scattered by the nanostructured surroundings into radiation that is detected as emission in the far field.

The work we report here is motivated by recent experiments where single or few molecules are embedded in submicron-sized host particles. These can be used as pointlike sources [2] or detectors [3] for high-resolution imaging of microstructures and optical fields. At low temperatures, the emitters are individually addressable in frequency space because their resonance frequencies sensitively depend on the local environment in the host particle. Previous work has shown that the emitters' spontaneous lifetime, which is independent of the illumination or detection mode, provides access to the dielectric surroundings on the nanometer scale if a single molecule is scanned over a structured substrate [4–7]. In a typical experiment, where the emitters are embedded in a small object, one can expect that the nanohost also has a strong impact on the molecular lifetime. This is the issue we analyze in this paper. The spontaneous emission rate is calculated for a pointlike dipole in a small, subwavelength dielectric host. Note that particles of such a small size do not support discrete modes, except the collective plasma oscillations for metallic particles. One therefore cannot expect the usual enhancement of the dipole emission in the vicinity of a Mie-like resonance. On the contrary, the field propagates in an almost static manner inside the host, since retardation is nearly negligible.

We present numerical calculations that are able to handle arbitrary orientations and positions of the dipole, as well as arbitrary host shapes and material. A large class of hosts from subwavelength to wavelength sized is covered as well. The smallest size our approach can describe is related to the validity of the macroscopic Maxwell equations: for hosts of typically a few atomic units in diameter or more, the response to an electric field can be described by an effective susceptibility instead of solving for a correlated few-electron quantum dynamics. The method we apply is based on the boundary integral formulation of the wave equation. It has been used for subwavelength optics problems with plane-wave illumination (see, e.g., [8,9]) and also for the determination of electron eigenmodes in quantum dots [10]. Very recently results for molecular emission outside a metallic nano-object have also been obtained with this method [11]. Our results compare favorably with analytical solutions for small elliptical particles that we obtain in the electrostatic approximation, neglecting retardation. We focus for numerical simplicity on a two-dimensional setting, but the good comparison we achieve between numerics and analytics leads us to believe that qualitatively similar trends will hold in three dimensions.

The paper is organized as follows. In Sec. II, we outline how classical electrodynamics permits the calculation of spontaneous decay rates and introduce the numerical method we use for the field computation. Section III discusses the relevance of the host shape and dipole position on the spontaneous decay rate. We explain in detail results summarized in a previous Letter [12] and compare to an analytical solution for elliptical particles. As an application interesting for apertureless SNOM, we discuss the case of molecular emit-

*Electronic address: Carsten.Henkel@quantum.physik.uni-potsdam.de

ters embedded in sharp tips (Sec. III C). Conclusions are presented in Sec. IV. The Appendixes collect technical material used in the text.

II. MODEL

A. Classical approach

In quantum mechanics, the spontaneous decay rate of an excited two-level system is given by Fermi's golden rule

$$\Gamma = \frac{2\pi}{\hbar^2}\sum_{\mathbf{k}\mu} |\langle g,1_{\mathbf{k},\mu}|\hat{\mathbf{p}}\cdot\hat{\mathbf{E}}(\mathbf{x}_s)|e,0\rangle|^2 \delta(\omega_{\mathbf{k},\mu}-\omega_{\mathrm{eg}}), \quad (1)$$

where $\hat{\mathbf{p}}$ is the electric dipole operator and $\hat{\mathbf{E}}(\mathbf{x}_s)$ the electric field operator, evaluated at the dipole's position $\mathbf{x}_s$. This formula shows explicitly that the excited state $|e\rangle$ dumps its energy $\hbar\omega_{\mathrm{eg}}$ into an empty mode of the vacuum field, creating one photon. The decay rate is the sum over all modes (with wave vector $\mathbf{k}$ and polarization μ). We assume in this paper that the spectral density of the field modes is sufficiently smooth so that the decay dynamics is characterized by the single rate Γ.

For a computation of the latter, it is actually not needed to perform an explicit mode expansion and quantization of the field. To show this, we recall that Eq. (1) can be written in the equivalent form [4,5,13–15]

$$\Gamma = \sum_{i,j} \frac{2p_i p_j^*}{\hbar}\,\mathrm{Im}\, G_{ij}(\mathbf{x}_s,\mathbf{x}_s;\omega_{\mathrm{eg}}), \quad (2)$$

where $\mathbf{p}=\langle g|\hat{\mathbf{p}}|e\rangle$ is the dipole matrix element and G_{ij} is the Green tensor whose imaginary part is related to the local density of states [4,16]. Consider now a classical dipole antenna with amplitude $\mathbf{p}(t)=\mathbf{p}e^{-\mathrm{i}\omega_{\mathrm{eg}}t}+\mathrm{c.c.}$ The electric field it creates is given in terms of the Green tensor as

$$E_{\mathrm{dip},i}(\mathbf{x},t) = E_{\mathrm{dip},i}(\mathbf{x})e^{-\mathrm{i}\omega_{\mathrm{eg}}t} + \mathrm{c.c.} = \sum_j G_{ij}(\mathbf{x},\mathbf{x}_s;\omega_{\mathrm{eg}})p_j + \mathrm{c.c.} \quad (3)$$

Applying Poynting's theorem and using Eqs. (2) and (3), one gets [15]

$$\frac{P_{\mathrm{em}}}{\hbar\omega_{\mathrm{eg}}} = \frac{2\,\mathrm{Re}[-\mathrm{i}\omega_{\mathrm{eg}}\mathbf{p}^*\cdot\mathbf{E}_{\mathrm{dip}}(\mathbf{x}_s)]}{\hbar\omega_{\mathrm{eg}}} = \Gamma, \quad (4)$$

where P_{em} is the total emitted power, averaged over one cycle of the dipole radiation—i.e., the integral of the Poynting vector over a large sphere in the far field. With the help of Eq. (4), we can thus compute the spontaneous decay rate in terms of the emission of a classical dipole by normalizing to the photon energy $\hbar\omega_{\mathrm{eg}}$.

We note that this approach works for absorptionless media. Otherwise, the power absorbed in the medium would appear as well in the Poynting theorem, Eq. (4). This contribution yields the rate of nonradiative decay, where the excited-state energy is absorbed in the medium without emission of a photon into the far field. The normalized far-field emission P_{em} gives the radiative decay rate in that case. The nonradiative decay rate diverges in a continuum description of an absorbing medium if the molecule is coupled to the electric field described by the macroscopic Maxwell equations [17–19]. The divergence can be regularized by introducing an empty bubble around the molecule, but the result depends sensitively on the bubble radius, a phenomenological parameter. To avoid this complication, we focus on nonabsorbing materials here.

When a molecular dipole is embedded in a dielectric host, one has in fact to take into account local field corrections that connect the "macroscopic" field $\mathbf{E}(\mathbf{x})$ to the "local" field at the position of the dipole. A common way to do this is the small bubble model mentioned before [20]. This is discussed in more detail in Appendix A where the local field correction for a nonabsorbing dielectric is shown to be equivalent to an "effective dipole moment," as also pointed out in [15]. We obtain results that are independent of the local field correction by normalizing the spontaneous decay rate to its value in a bulk dielectric, where the same correction applies. (For the case of an absorbing medium, see [21].)

B. Basic equations

The numerical solution of Maxwell's equation in a dielectric of arbitrary shape is quite efficiently obtained in a geometry that is invariant along one axis (cylindrical objects) because the problem then reduces effectively to a two-dimensional one. The nanohost is modeled as a linear, isotropic, homogeneous, and nonmagnetic medium with dielectric function $\varepsilon(\omega)$ in its interior. We focus on the case that the molecular dipole moment is oriented in the computational plane (p polarization). The other case (s polarization) would correspond to a completely different physical situation (an infinitely long, oscillating current) whose near-field behavior has not much to do with the emission from a dipole source. In p polarization, the Maxwell equations imply that the magnetic field has only one nonvanishing component $H(\mathbf{r})=H(x,y)$ so that we deal with a scalar problem. In the following, all vectors (except $\mathbf{e}_z$) are two dimensional. The wave equation for the magnetic field reads

$$\boldsymbol{\nabla}\cdot\frac{1}{\varepsilon(\mathbf{r})}\boldsymbol{\nabla}H + k^2 H = \frac{\mathrm{i}\omega}{\varepsilon(\mathbf{x}_s)}\mathbf{p}\cdot(\hat{\mathbf{e}}_z\times\boldsymbol{\nabla})\delta(\mathbf{r}-\mathbf{x}_s), \quad (5)$$

where $\mathbf{x}_s$ is the dipole position. We write $\omega=\omega_{\mathrm{eg}}$ for simplicity and use the vacuum wave number $k=\omega/c$. Across the surface of the dielectric object, the field H and the tangential component of the electric field, $F=(1/\varepsilon)(\partial H/\partial n)$, are continuous, where $\partial/\partial n$ is the derivative along the outward normal.

To solve the partial differential equation (5), we transform it into a boundary integral equation using the Green theorem as explained in [22]. For a point $\mathbf{r}$ in the interior $\mathcal{D}$ of the object, we get

$$H_{\mathrm{int}}(\mathbf{r}) = H_{\mathrm{dip}}(\mathbf{r}) + \int_{\partial\mathcal{D}} d\sigma(\mathbf{x})\left[G_\varepsilon(\mathbf{x}-\mathbf{r})\frac{\partial H}{\partial n}(\mathbf{x}) - H(\mathbf{x})\frac{\partial G_\varepsilon}{\partial n}(\mathbf{x}-\mathbf{r})\right], \quad (6)$$

$$H_{\mathrm{dip}}(\mathbf{r}) = \mathrm{i}\omega(\mathbf{p}\times\hat{\mathbf{e}}_z)\cdot\boldsymbol{\nabla}\, G_\varepsilon(\mathbf{x}_s-\mathbf{r}), \tag{7}$$

$$G_\varepsilon(\mathbf{r}) = \frac{\mathrm{i}}{4}H_0^{(1)}(kr\sqrt{\varepsilon}), \tag{8}$$

where $\partial\mathcal{D}$ is the inner side of the object boundary, $\mathrm{d}\sigma(\mathbf{x})$ is the (scalar) surface element at the integration point $\mathbf{x}$, and G_ε is the retarded Green function for a homogeneous dielectric involving the zeroth-order Bessel function of the third kind $H_0^{(1)}$, henceforward denoted as H_0. Equation (6) implements the natural separation of the interior field into the dipole field $H_{\mathrm{dip}}(\mathbf{r})$ for an infinite dielectric and a field reflected from the object boundary. Similarly, outside the object the field is

$$H_{\mathrm{ext}}(\mathbf{r}) = -\int_{\partial\mathcal{D}} d\sigma(\mathbf{x})\left[G_1(\mathbf{x}-\mathbf{r})\frac{\partial H}{\partial n}(\mathbf{x}) - H(\mathbf{x})\frac{\partial G_1}{\partial n}(\mathbf{x}-\mathbf{r})\right], \tag{9}$$

where G_1 is the Green function for vacuum. From Eqs. (6) and (9), the field is completely determined by the field and its derivative on the boundary (Huyghens principle). Note that the exterior field automatically satisfies the Sommerfeld radiation condition at infinity due to the choice of the retarded Green function.

The field (and its normal derivative) on the boundary are fixed self-consistently by letting the observation point $\mathbf{r}$ approach the boundary in Eqs. (6) and (9). One has to take care of the nonintegrable singularity in the Green function's derivative, as explained in Appendix B. In terms of the fields H and F which take the same value on both sides of the interface, we find the inhomogeneous boundary integral equations

$$H(\mathbf{r}) = 2H_{\mathrm{i}}(\mathbf{r}) + 2\mathrm{P}\int_{\partial\mathcal{D}} d\sigma(\mathbf{x})\left[G_\varepsilon(\mathbf{x}-\mathbf{r})\varepsilon F(\mathbf{x}) - H(\mathbf{x})\frac{\partial G_\varepsilon}{\partial n}(\mathbf{x}-\mathbf{r})\right], \tag{10}$$

$$H(\mathbf{r}) = -2\mathrm{P}\int_{\partial\mathcal{D}} d\sigma(\mathbf{x})\left[G_1(\mathbf{x}-\mathbf{r})F(\mathbf{x}) - H(\mathbf{x})\frac{\partial G_1}{\partial n}(\mathbf{x}-\mathbf{r})\right], \tag{11}$$

where P denotes a principal value prescription, excluding the singular part of $\partial G_\varepsilon/\partial n$. The logarithmic singularity of the Green function itself when $\mathbf{x}\to\mathbf{r}$ can be treated by singling out a small neighborhood σ around the surface point $\mathbf{r}$, along the method outlined in Appendix B. Its contribution to the integral is then

$$\int_\sigma d\sigma(\mathbf{x})G_\varepsilon(\mathbf{x}-\mathbf{r})\varepsilon F(\mathbf{x}) \approx \sigma\varepsilon F(\mathbf{r})[-2\gamma + \mathrm{i}\pi + 2 - 2\ln(k\sigma\sqrt{\varepsilon}/4)]. \tag{12}$$

For the numerical solution, we apply the method of moments [23]: the boundary is discretized into segments of size $\mathrm{d}\sigma$ and the integrals are approximated by Riemann sums. The corners of polygonal objects are smoothed. The integral equation is evaluated at discrete points centered in the segments (point matching), and each point $\mathbf{r}_j$ carries two unknowns $H_j=H(\mathbf{r}_j)$ and F_j. The integral equations (10) and (11) are thus replaced by a linear system that is solved with standard routines. To get converged results, we choose $\mathrm{d}\sigma$ a factor of 10 smaller than the minimum of the local wavelength $\lambda/\sqrt{\varepsilon}$ and the minimum distance of the dipole to the boundary. The emitted power is computed from Eq. (9) with $\mathbf{r}$ in the far field. We use the corresponding expansion of the Green function and perform the angular integral of the Poynting vector numerically.

C. Validation of numerical results

We have validated the numerical results by comparing them to analytical calculations in the exactly solvable case of a circular object surrounded by vacuum. A dipole at the center of the object creates the dipole field

$$H_{\mathrm{dip}}(\mathbf{r}) = -\frac{\omega kp\sqrt{\varepsilon}\sin\psi}{4}H_1(kr\sqrt{\varepsilon}), \tag{13}$$

where ψ is the angle between $\mathbf{r}$ and the dipole and H_1 the first-order Bessel function. This would also be the field in a bulk dielectric. Outside the object, the field is $H_{\mathrm{ext}}=tH_{\mathrm{dip}}$, where the transmission coefficient can be found by a calculation similar to the Mie solution in three dimensions [24]:

$$t = -\frac{2\mathrm{i}/(\pi ka\sqrt{\varepsilon})}{H_1(ka)J_1'(ka\sqrt{\varepsilon}) - \sqrt{\varepsilon}H_1'(ka)J_1(ka\sqrt{\varepsilon})}. \tag{14}$$

Here, a is the object radius and the prime denotes the derivative with respect to the argument. The normalized power emitted by the dipole is found to be

$$\frac{P_{\mathrm{em}}}{P_{\mathrm{bulk}}} = \frac{\Gamma}{\Gamma_{\mathrm{bulk}}} = |t|^2. \tag{15}$$

For a dielectric host particle, this is plotted as a solid line in Fig. 1. The dipole emission wavelength $\lambda=2\pi c/\omega$ is scanned through a wide range from $\lambda\sim a$ to much smaller than the particle radius. The numerical data are shown by the symbols and are in good agreement. As the number of boundary elements increases, the relative error of the numerical solution decreases rapidly; see the inset of Fig. 1.

As a second example, we consider the scattering cross section for a cylindrical metallic particle illuminated by a plane wave. The numerical data shown in Fig. 2 agree quite well with the results of Mie theory [24]. The convergence with the number of boundary elements (inset of Fig. 2) is somewhat slower, probably due to the faster variations of the field inside the metal particle. Note that we use the dielectric function tabulated in [25]; there is no need to assume a particular analytical form for $\varepsilon(\omega)$ as would be required for an integration in the time domain.

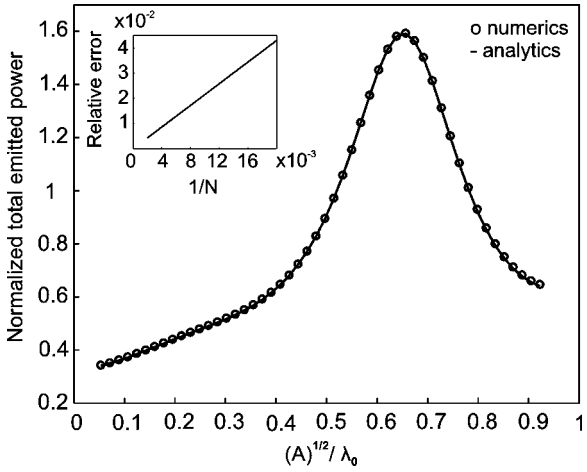

FIG. 1. Emission from a dipole centered in a circular object: normalized total emitted power $P_{\mathrm{em}}/P_{\mathrm{bulk}}$ vs emission frequency. Symbols: numerical results. Solid line: analytical results based on Eqs. (14) and (15). Inset: test of convergence. The relative error of the decay rate is plotted vs the inverse number $1/N$ of boundary elements. An error smaller than 1% is achieved for $N>250$. Parameters: dielectric cylinder with $\varepsilon=2.5$, surrounded by vacuum. The results of the main figure are obtained with $N=300$ boundary elements. For the inset, emission wavelength $\lambda_0=525$ nm and cylinder radius $a=30$ nm.

III. RESULTS AND DISCUSSION

A. Polygonal hosts

1. Spontaneous decay rate

We plot in Fig. 3 the normalized emitted power $P_{\mathrm{em}}/P_{\mathrm{bulk}}=\Gamma/\Gamma_{\mathrm{bulk}}$ for a molecule located in dielectric host

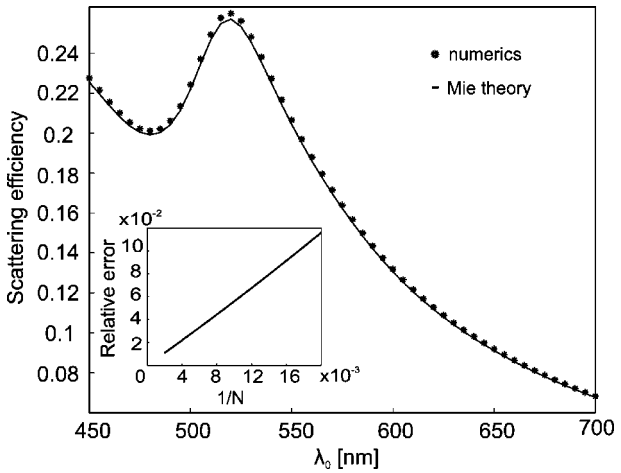

FIG. 2. Scattering cross section for a metallic cylinder: comparison of Mie theory and numerical results. We plot the scattering cross section normalized to the particle diameter. Inset: relative error between the numerical and analytical values of the scattering cross section versus the inverse number $1/N$ of boundary elements. Above $N=400$ points, a relative error $<1\%$ is achieved. Parameters: *p*-polarized incident plane wave with tunable wavelength, gold cylinder of radius $a=30$ nm, surrounded by vacuum. The dielectric function is taken from [25]. $N=500$ boundary elements are taken in the main figure. In the inset, $\lambda_0=525$ nm.

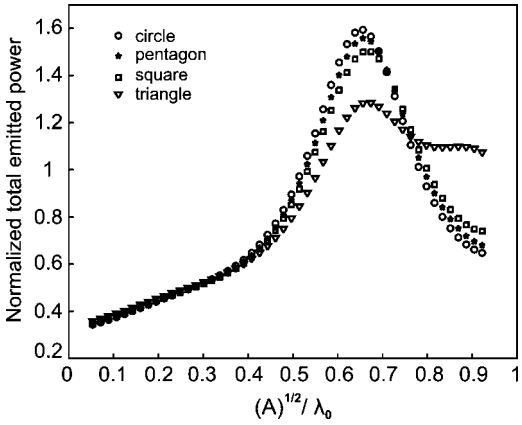

FIG. 3. Radiative decay rate vs emission frequency for host particles of the same area and aspect ratio, but with different shapes. Parameters: tunable *p*-polarized dipole located at the object center, dielectric object ($\varepsilon=2.5$) surrounded by vacuum. The wavelength is normalized to the square root of the particle area, the decay rate normalized to its value in a bulk dielectric.

particles of different size and shape. The molecule is located at the object center, and its emission wavelength is varied. One observes a broad peak located at the object's first Mie resonance. For a circular shape, this resonance corresponds to the smallest complex zero of the denominator in Eq. (14). It is apparent that the object shape does not significantly shift the position of the peak; only its amplitude is reduced for polygons that differ strongly from a circle. One also notices that inside a very small object, the radiative lifetime approaches a common limit independent of the shape. This limit is in agreement with the small-size limit of Eqs. (14) and (15):

$$\lim_{ka\ll 1}\frac{\Gamma}{\Gamma_{\mathrm{bulk}}}=\left(\frac{2}{\varepsilon+1}\right)^2. \tag{16}$$

We notice that the emission is weaker than inside a homogeneous dielectric (unless $-3<\varepsilon<1$, we do not consider this range here). This can be attributed to the screening of the molecular dipole by the polarization charges it induces on the object surface. As a result, the far field contains a reduced dipole component. We give a more detailed discussion in Sec. III B 2 below where elongated shapes are considered, too.

In a previous Letter, we have also shown that the dependence on the dipole position inside polygonal hosts is relatively weak [12]. For a circular particle and in the quasistatic limit, the decay rate is strictly constant, and any deviation can be attributed to retardation. For polygonal particles, an enhanced decay is only observed if the molecule approaches sharp corners, due to the stronger electrostatic fields there [26]. We discuss another example in Sec. III C below where the host is a sharp tip.

2. Radiation pattern

In Fig. 4, we plot the angular distribution of the emission (radiation pattern) for a molecule embedded in two square hosts that have dimensions either smaller or larger than a

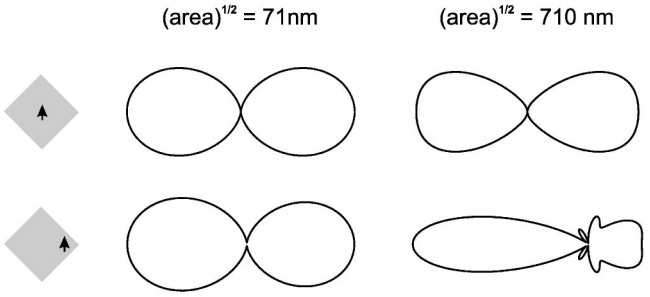

FIG. 4. Radiation pattern for a molecule in polygonal hosts smaller and larger, respectively, than the wavelength. Parameters: square hosts with areas as indicated, $\varepsilon=2.5$, emission wavelength $\lambda_0=600$ nm. The molecule position in the particle and its dipole moment are indicated on the left.

wavelength. This pattern is computed from the far-field expression

$$\frac{1}{P_{\text{bulk}}}\frac{dP_{\text{em}}}{d\theta}=\lim_{r\to\infty}\frac{r}{2\pi^2\omega^2kp^2}|H(\mathbf{r})|^2. \tag{17}$$

We observe in the figure that the emission essentially resembles the familiar dipole pattern for the subwavelength host and does not depend on the dipole position. Significant structure occurs for objects comparable to or larger than the wavelength: with the emitter at the center, the angular distribution changes only slightly, while pronounced lobes appear with an off-centered source. This confirms the approach of Klimov, Ducloy, and Letokhov [27] who relate the emitted power to the effective dipole moment p_{eff} that the molecule induces in a subwavelength object, $ka\ll 1:\Gamma/\Gamma_{\text{bulk}}\to|p_{\text{eff}}/p|^2$. Higher multipoles apparently make a negligible contribution to the radiated field in this case. (For the small object in Fig. 4, $kA^{1/2}\approx 0.74$ with A the object area.) Figure 3 shows, however, that the decay rate rapidly deviates from its electrostatic limit, with an approximately linear increase with $kA^{1/2}$, in agreement with the perturbation expansion of [28].

B. Elongated hosts

1. Spontaneous decay rate and field distributions

More pronounced changes in the radiative lifetime are found for elongated host particles, as shown in Fig. 5. The emission peaks now depend on the aspect ratio of the object. This behavior can be attributed to a standing-wave mode of low order that the dipole excites. An example is visible in the field intensity map plotted in Fig. 6. Because of the low index contrast considered here, the confinement of the field inside the particle is weak. The modes thus have a low quality factor, and the emission resonances are broad, as was also seen in Fig. 3.

In the limit of dielectric particles that are very small compared to the (medium) wavelength, this picture does not apply any longer since the particle does not support any mode. In this regime, electrostatic arguments permit to understand the dependence of the spontaneous decay rate on the object's aspect ratio and orientation of the dipole. We show in particular that screening due to induced surface charges qualitatively explains the numerical results.

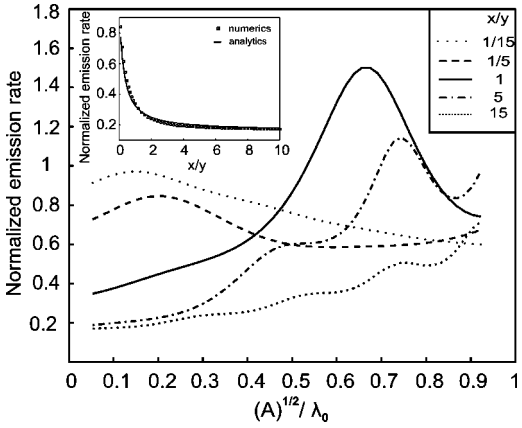

FIG. 5. Same as Fig. 3 for rectangular hosts of different aspect ratio x/y. Parameters: tunable p-polarized dipole at object center, dielectric object ($\varepsilon=2.5$) surrounded by vacuum. Inset: decay rate for very small objects vs aspect ratio. Numerical data are for nanoscopic rectangular objects ($\sqrt{A}=0.01\lambda_0$), analytical data for elliptic objects in the electrostatic limit [Eq. (18)].

2. Screening

The charge density induced on the surface of a typical rectangular object is plotted in Fig. 7. It is well known from electrostatics that the object shape influences the charge distribution. For the special case of an elliptical object, the electrostatic problem of an embedded point dipole can be solved analytically, as we outline in Appendix C. If the dipole is polarized along one axis of the ellipse (length c), the far field corresponds to a screened dipole moment $p_{\text{eff}}=f_c\,p$ where the depolarization factor f_c is given in Eq. (C8). With this effective dipole moment, we get a decay rate

$$\frac{\Gamma}{\Gamma_{\text{bulk}}}=|f_c|^2=\frac{1}{[1+(\varepsilon-1)b/(b+c)]^2}, \tag{18}$$

where b is the other ellipse axis. This formula reproduces the correct value (16) for a circular object. It is also in good agreement with the numerical results obtained for small rect-

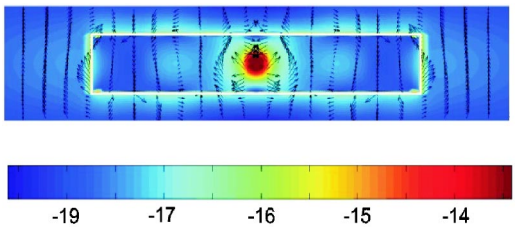

FIG. 6. (Color online) Field intensity created inside an elongated host by a single dipole source (dipole moment pointing upwards). The color code gives the field intensity $|\mathbf{E}(\mathbf{x})|^2$ (color bar in logarithmic scale) in arbitrary units: the arrows illustrate the electric field Re $\mathbf{E}$ in phase with the source. The chosen host corresponds to maximum emission for aspect ratio $x/y=5$ in Fig. 5: rectangle with size (1006.2×201.24) nm^2, $\varepsilon=2.5$, wavelength $\lambda_0=600$ nm.

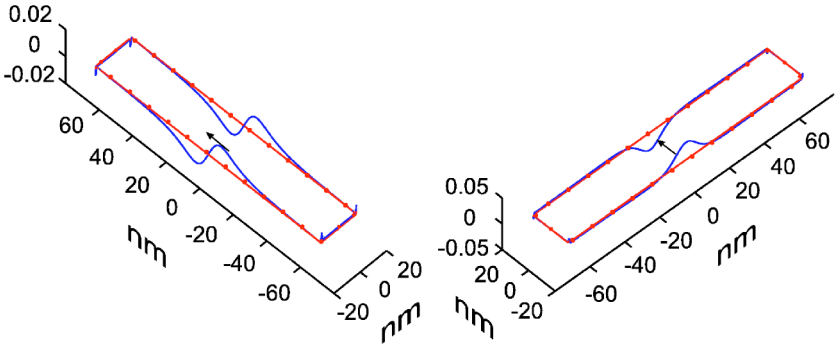

FIG. 7. (Color online) Surface charge density (in arbitrary units) induced on the surface of an elongated rectangular host, for two orientations of the molecular dipole moment. Blue curves: charge density in phase with the dipole. Red curves with dots: charge density in phase quadrature.

angular objects, as shown in the inset of Fig. 5. For very elongated objects, we have

$$b \ll c\text{: } \Gamma = \Gamma_{\text{bulk}}, \tag{19}$$

$$b \gg c\text{: } \Gamma = \Gamma_{\text{bulk}}/\varepsilon^2, \tag{20}$$

which is similar to the behavior of fluorescence from thin dye films [29]. An intuitive explanation is based on Fermi's golden rule (1) and the penetration of the vacuum field modes into the object: in the first case, dipole and field are tangential to the film and the field is continuous across the film surface. In the second case, the dipole is perpendicular to the film, and the corresponding vacuum mode is reduced, inside the film, by a factor of $1/\varepsilon$ because now the displacement field $D=\varepsilon E$ is continuous across the surface.

C. Molecules embedded in dielectric tips

We finally consider elongated particles in order to gain insight into the impact of the tip geometry on the spontaneous emission of a molecule embedded in the tip. Figure 8 illustrates, for a fixed distance of the molecule from the tip apex, the dependence on the sharpness of an elliptical tip. A significant enhancement of the decay rate is found for very sharp tips, due to strong electrostatic fields and large induced surface charges. In Fig. 9, a triangular host object is considered as an extreme case. Again, the decay rate increases as the molecule approaches the apex of the triangle. The field distribution for two generic molecule positions is plotted in Fig. 10: close to the apex, the dipole creates a field that is strongly localized on a scale of some 10 nm. The energy flow (Poynting vector), indicated by the field lines, suggests that the tip redirects the emission in the upward direction, along the faces of the triangle. This agrees with the fact that close to a planar dielectric, most of the emission goes into modes that are evanescent in vacuum and propagate just beyond the critical angle inside the dielectric (see, e.g., [30,31]).

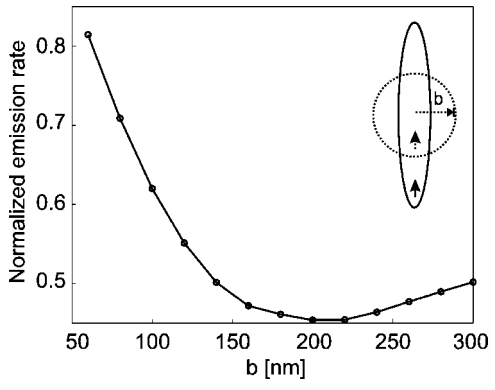

FIG. 8. Impact of tip sharpness: radiative decay rate in elliptical dielectric hosts with different aspect ratio. The dipole is situated in all cases at a fixed distance 30 nm from the tip apex, with vertical dipole moment. Emission wavelength $\lambda_0=600$ nm, fixed host area $(600\text{ nm})^2$, $\varepsilon=2.5$, surrounded by vacuum.

IV. CONCLUSIONS AND OUTLOOK

Based on the boundary integral equation method for the solution of the Maxwell equations, we have developed in this paper a versatile numerical method to compute the spontaneous emission rate of an emitter embedded in a (lossless) dielectric host particle of arbitrary shape and a size comparable to or smaller than the emission wavelength. We have found that compared to the decay rate in a bulk dielectric, significant modifications occur for elongated hosts with subwavelength size. The general features of our results can be understood from electrostatic arguments in terms of a screened effective dipole moment, confirming the picture put forward by Klimov, Ducloy, and Letokhov [27]. Our numerical calculations have allowed to assess the validity of this approximation. If the molecule is located close to sharp corners, the

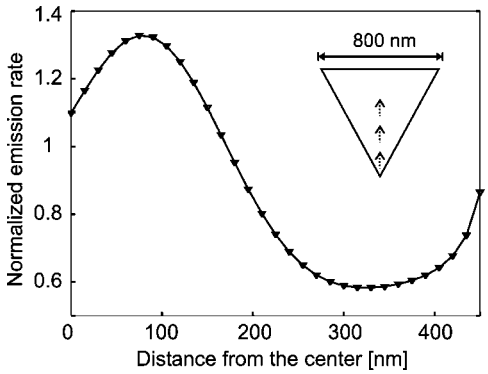

FIG. 9. Molecule close to a triangular tip: radiative decay rate vs source position in an equilateral triangle. Vertical dipole emitting at $\lambda_0=600$ nm, host dimensions as indicated in the inset, $\varepsilon=2.5$, surrounded by vacuum.

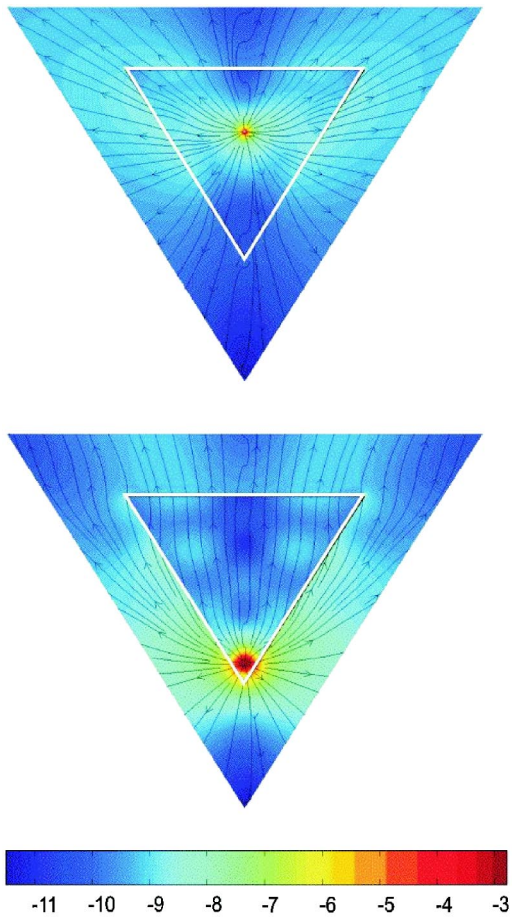

FIG. 10. (Color online) Intensity distribution inside a triangular host created by a vertical point dipole. Vertical dipole with emission wavelength $\lambda_0=600$ nm. Dielectric particle with $\varepsilon=2.5$, base length=800 nm, surrounded by vacuum. The intensity distribution (color bar in logarithmic scale) and the time-averaged energy flow (given by the arrows) are plotted for a centered and an off-centered dipole, respectively.

decay rate is enhanced because of the lightning rod effect. An exact electrostatic solution for elliptical particles gives a satisfactory description for the emission out of rectangular hosts of very small size as well. With the small refractive index contrast we consider here, eigenmodes of the particle have low quality factors and give only broad resonances when the particle size becomes comparable to the wavelength.

The boundary integral equation can be adapted to take into account a planar substrate, simply by using the appropriate Green function [32,33]. Corrugations are then modeled as finite objects, without the need to truncate the substrate. This would allow to study in detail the validity of the perturbative calculation done in [5,6].

ACKNOWLEDGMENTS

L.R. thanks Vahid Sandoghdar for supervising her research and suggesting the routes explored in this work. We are indebted to Hannes Schniepp, Rémi Carminati, Sven Burger, Achim Schädle, and Frank Schmidt for fruitful comments. C.H. thanks Martin Wilkens for continuous support. This work has been supported by the Deutsche Forschungsgemeinschaft in the framework of the Schwerpunktprogramm 1113 "Photonic Crystals."

APPENDIX A: LOCAL FIELD CORRECTIONS

We discuss here the decay rate of a two-level system embedded in a lossless, two-dimensional dielectric object. A quantization scheme for the macroscopic field is used and local field corrections are analyzed.

1. Homogeneous dielectric

Using a mode expansion of the field, the matrix element in Fermi's golden rule (1) can be evaluated as

$$|\langle g,1_{\mathbf{k},\mu}|\hat{\mathbf{p}}\cdot\hat{\mathbf{E}}(\mathbf{x}_s)|e,0\rangle|^2=\frac{\hbar\omega_{\mathbf{k},\mu}}{2\varepsilon_0\varepsilon L\Omega}|\mathbf{p}^*\cdot\mathbf{f}^{\mathrm{loc}}_{\mathbf{k},\mu}|^2, \quad \text{(A1)}$$

where $\Omega(L)$ is the quantization area (length) in the xy plane (the z axis), respectively. The field modes are labeled by the wave vector $\mathbf{k}$ and the polarization index μ, and $\mathbf{f}^{\mathrm{loc}}_{\mathbf{k},\mu}$ is the actual (local) field at the location of the molecule. The factor $1/\varepsilon$ in the electric field per photon comes from the expression for the electromagnetic energy density $(\varepsilon\varepsilon_0/2)\mathbf{E}^2+\mathbf{B}^2/(2\mu_0)$ in a (nondispersive) dielectric.

The local field is related by a "depolarization factor" ξ_μ to the "macroscopic field":

$$\mathbf{f}^{\mathrm{loc}}_{\mathbf{k},\mu}=\xi_\mu\mathbf{f}_{\mathbf{k},\mu}(\mathbf{x}_s). \quad \text{(A2)}$$

We anticipate a polarization dependence, but no strong variation with the wave vector for the local field correction. This would no longer be true in a birefringent host particle, for example. In fact, ξ_μ is determined by the microscopic surroundings of the molecule that typically vary on a scale much shorter than the wavelength. For the calculation of ξ_μ, retardation can thus be neglected, and one faces an electrostatic problem where $\mathbf{f}_{\mathbf{k},\mu}(\mathbf{x})$ can be approximated by an external, quasihomogeneous field [26]. We do not need an actual formula for ξ_μ here; it can be found by adapting the result given in Eq. (A5). For the three-dimensional case, see, e.g., [17,18,21,34].

In our two-dimensional model, only wave vectors $\mathbf{k}$ in the plane are retained and are specified by an angle φ with respect to the dipole moment $\mathbf{p}$ (assumed in the plane as well). Then only p-polarized modes (electric field in the plane) contribute to Eq. (A1) with a matrix element proportional to $\sin\varphi$. Performing the angular integral, the decay rate becomes

$$\Gamma_{\mathrm{bulk}}=\frac{|\xi_p\mathbf{p}|^2}{4\varepsilon_0\hbar L}\frac{\omega_{\mathrm{eg}}^2}{c^2}. \quad \text{(A3)}$$

The local field correction thus enters quadratically into the decay rate and could as well be absorbed in a redefinition of the dipole moment $\mathbf{p}$. We have assumed an isotropic local field correction here (molecule in a circular cavity). That Eq. (A3) does not depend any longer explicitly on ε is typical for

a two-dimensional setting, as has been shown by Nienhuis and Alkemade [35]. In fact, the factor $1/\varepsilon$ in Eq. (A1) is compensated by a factor of ε that occurs in the density of modes for a two-dimensional, homogeneous dielectric with dispersion relation $\omega_{\mathbf{k},\mu}=c|\mathbf{k}|/\sqrt{\varepsilon}$.

2. Small ellipsoidal object

We now turn to a dipole inside a finite dielectric object of subwavelength size. In this case, we use scattering mode functions $\mathbf{f}_{\mathbf{k},\mu}(\mathbf{x})$ that are labelled by plane waves $\mathbf{e}_{\mathbf{k},\mu}e^{i\mathbf{k}\cdot\mathbf{x}}$ incident from vacuum on the object. The quantization area Ω is much larger than the object, so that the latter does not affect the normalization of the mode functions. We thus get the matrix element

$$|\langle g,1_{\mathbf{k},\mu}|\hat{\mathbf{p}}\cdot\hat{\mathbf{E}}(\mathbf{x}_s)|e,0\rangle|^2=\frac{\hbar\omega_{\mathbf{k},\mu}}{2\varepsilon_0 L\Omega}|\mathbf{p}^*\cdot\mathbf{f}^{\mathrm{loc}}_{\mathbf{k},\mu}|^2, \tag{A4}$$

instead of Eq. (A1), and the mode frequency $\omega_{\mathbf{k},\mu}=ck$ does not contain ε.

To get the field inside the object, we use again an electrostatic argument given that the dielectric particle is small compared to the wavelength: we solve the classical problem of a small ellipsoid in an external homogeneous electric field (given by the polarization vector $\mathbf{e}_{\mathbf{k},\mu}$). The exterior field contains scattered dipole and multipole fields in addition to the external field. The interior field, for an elliptical shape, is again homogeneous with an amplitude given by the depolarization factor [36]

$$f^{\mathrm{int}}_{\mathbf{k}\mu,\alpha}=\frac{1}{1+(\varepsilon-1)n_\alpha}f_{\mathbf{k},\mu,\alpha}\equiv\tau_\alpha f_{\mathbf{k},\mu,\alpha}(\mathbf{x}_s), \tag{A5}$$

where α labels the Cartesian components in a frame given by the ellipsoid's principal axes. In this frame, the depolarization is described by the numbers n_α. For a cylinder with elliptical cross section (axes b,c), the three-dimensional results of Ref. [36] lead to $n_c=b/(b+c)$, $n_b=c/(b+c)$. This in agreement with the solution of Appendix C for the reciprocal situation (the exterior dipole field created by a dipole embedded in an ellipsoid). Finally, the components of the local field are found from the field inside the object applying the same correction factor, $f^{\mathrm{loc}}_{\mathbf{k}\mu,\alpha}=\xi_\mu f^{\mathrm{int}}_{\mathbf{k}\mu,\alpha}$. This assumes that the microscopic surroundings of the molecule are the same in the object and in bulk.

For an elliptical object, we have to take into account the dependence of the depolarization on the orientation of the field polarization. Expanding an in-plane dipole moment along the principal axes, $\mathbf{p}=p_b\mathbf{e}_b+p_c\mathbf{e}_c$, we have, for a given p-polarized mode,

$$\mathbf{p}^*\cdot\mathbf{f}^{\mathrm{loc}}_{\mathbf{k},p}=\xi_p(p_b^*\tau_b\mathbf{e}_b+p_c^*\tau_c\mathbf{e}_c)\cdot\mathbf{f}_{\mathbf{k},p}(\mathbf{x}_s), \tag{A6}$$

where we have again assumed an "isotropic" local field correction ξ_p. The integration over the angle φ between $\mathbf{k}$ and $\mathbf{e}_b$ gives

$$\int_0^{2\pi}d\varphi|p_b\tau_b\sin\varphi+p_c\tau_c\cos\varphi|^2=\pi(p_b^2\tau_b^2+p_c^2\tau_c^2); \tag{A7}$$

the mixed terms cancel. We finally get a decay rate

$$\Gamma_{\mathrm{object}}=\Gamma_{\mathrm{bulk}}(\tau_b^2\cos^2\phi+\tau_c^2\sin^2\phi), \tag{A8}$$

where ϕ is the angle of the dipole with respect to the b axis. If the dipole is polarized along one of the axes of the ellipsoid, we get a decay rate proportional to the corresponding depolarization factor. For an orientation in between, one has a contribution of both. Finally, the local field correction ξ_μ [involved in Γ_{bulk}, Eq. (A3)] drops out when normalizing the decay rate (A8) to its bulk value.

APPENDIX B: BOUNDARY INTEGRAL EQUATIONS

In Eqs. (6) and (9), the Green functions $G_\varepsilon(\mathbf{r}-\mathbf{x})$ and $G_1(\mathbf{r}-\mathbf{x})$ are singular in the limit $\mathbf{r}\to\mathbf{x}$. This does not pose problems in the far field, $\mathbf{r}\to\infty$, because $\mathbf{x}$ runs over the object boundary ∂D. But the boundary integral equations (10) and (11) require some care because, here, $\mathbf{r}\in\partial D$.

The derivative $\partial G_\varepsilon/\partial n$ contains a δ-function singularity. To extract it, we introduce for $\mathbf{r}\to\partial D$ a local coordinate system $\mathbf{r}=(x,h)$, $\mathbf{x}=(x_1,0)$ where h measures the distance of $\mathbf{r}$ from the surface in the direction of the outward unit normal. The boundary integral in the neighborhood $\sigma(\mathbf{r}_0)$ of the projection $\mathbf{r}_0=(x,0)$ onto the surface is then approximated by using the asymptotic expansion of the Bessel function. This leads to (see, e.g., [37])

$$\begin{aligned}\lim_{\mathbf{r}\to\partial D}\int_{\sigma(\mathbf{r}_0)}d\sigma(\mathbf{x})H(\mathbf{x})\frac{\partial G_\varepsilon}{\partial n}(\mathbf{x}-\mathbf{r})&=\frac{1}{2\pi}\lim_{h\to0}\int_{\sigma(\mathbf{r}_0)}dx_1H(\mathbf{x})\frac{h}{h^2+(x_1-x)^2}\\&=\frac{1}{2}\int_{\sigma(\mathbf{r}_0)}dx_1H(\mathbf{x})\delta(x_1-x)\mathrm{sgn}\,h=-\frac{H(\mathbf{r}_0)}{2}.\end{aligned} \tag{B1}$$

In the last step, we have used the Lorentzian representation of the δ function and assumed that the boundary ∂D is approached from inside the object ($h<0$). Equation (B1) leads to the factor of 2 in front of the boundary integrals in Eqs. (10) and (11).

The term involving $G_\varepsilon(\mathbf{r}-\mathbf{x})$ shows a logarithmic singularity. Extracting it in a similar way, the neighborhood $\sigma(\mathbf{r}_0)$ yields the contribution given in Eq. (12).

The linear system that represents the boundary integral equations on a discrete set of N surface elements corresponds to a matrix with N^2 entries. The computation of the matrix elements and the solution of the linear system on a workstation takes roughly 10 s for $N\approx500$. Reasonably converged results are obtained for $N\geqslant100$, as illustrated in Figs. 1 and 2.

APPENDIX C: EXACT SOLUTION FOR SUBWAVELENGTH ELLIPTIC OBJECT

We outline in the following the analytical solution for the electrostatic field created by a point dipole at the centre of an elliptical object. On the subwavelength scale, retardation is negligible so that we have to solve the generalized Laplace equation

$$\varepsilon_0 \nabla \cdot \varepsilon(\mathbf{r}) \nabla U = (\mathbf{p} \cdot \nabla) \delta(\mathbf{r}), \tag{C1}$$

where U is the electric (scalar) potential.

The Laplace equation (C1) can be separated in spheroidal coordinates defined by

$$x = l \sinh \rho \cos \varphi, \tag{C2}$$

$$y = l \cosh \rho \sin \varphi, \tag{C3}$$

where l is a length scale parameter. The surface of the elliptical object is the curve $\rho = \rho_0$, with the major axis $b = l \cosh \rho_0$ oriented along the y axis and the minor axis $c = l \sinh \rho_0$ along the x axis. The scale parameter is fixed by $l^2 = b^2 - c^2$. In these coordinates, the electrostatic potential of a point dipole polarized along the x axis in a homogeneous medium of permittivity ε is given by

$$U_{\mathrm{dip}} = \frac{p_x}{2\pi\varepsilon_0\varepsilon} \frac{\partial}{\partial x} \ln|\mathbf{x}| = \frac{p_x}{2\pi\varepsilon_0\varepsilon l} \frac{\sinh \rho \cos \varphi}{\cosh^2 \rho - \cos^2 \varphi}. \tag{C4}$$

The main complication here is that this potential does not depend in a simple way on the angular coordinate φ.

We add to Eq. (C4) a solution of the homogeneous Laplace equation $(\partial^2/\partial\rho^2 + \partial^2/\partial\varphi^2)U = 0$ in order to satisfy the boundary conditions. Those homogeneous solutions that are adapted to the symmetry of the present problem (even in φ) are of the following form. Outside the object,

$$U_{\mathrm{ext}} = \sum_{n=1}^{\infty} c_n \exp(-n\rho)\cos(n\varphi). \tag{C5}$$

The term with $n = 1$ is the dipole component and contains the effective dipole moment that we are looking for. For the interior field, we have the expansion

$$U_{\mathrm{int}} = U_{\mathrm{dip}} + \sum_{n=1}^{\infty} a_n \sinh(n\rho)\cos(n\varphi). \tag{C6}$$

The coefficients a_n and c_n are found from the continuity of the scalar potential across the boundary and the jump of its normal derivative, $\varepsilon \partial U_{\mathrm{int}}/\partial\rho = \partial U_{\mathrm{ext}}/\partial\rho$, at $\rho = \rho_0$. We expand these equations in a cosine Fourier series and find, performing one Fourier integral, the coefficient of the exterior dipole field:

$$c_1 = \frac{p_x/(\varepsilon_0 \pi l)}{1 + (\varepsilon - 1)\cosh \rho_0 e^{-\rho_0}}. \tag{C7}$$

In terms of the semiaxes of the ellipse, we have $e^{\rho_0} = \cosh \rho_0 + \sinh \rho_0 = (b + c)/l$. By comparing to the far field of a dipole in vacuum [Eq. (C4) in the limit of large ρ, with p_{eff} instead of p_x/ε], we get the effective dipole moment

$$p_{\mathrm{eff}} = \frac{p_x}{1 + (\varepsilon - 1)b/(b + c)}. \tag{C8}$$

One has to exchange b and c if the dipole is polarized along the y axis. For a circular cylinder, we have $b = c$ and get the known result $p_{\mathrm{eff}}/p_x \to 2/(\varepsilon + 1)$, leading to Eq. (16). For $\varepsilon \to -1$, the dipole excites a surface plasmon resonance and the solution diverges, unless damping is taken into account. For an elliptical particle, the resonance shifts to $\varepsilon = -c/b$; a similar trend has been observed in three dimensions by [38,39], for example.

[1] R. C. Dunn, Chem. Rev. (Washington, D.C.) **99**, 2891 (1999).
[2] J. Michaelis, C. Hettich, J. Mlynek, and V. Sandoghdar, Nature (London) **405**, 325 (2000).
[3] J. Michaelis, C. Hettich, A. Zayats, B. Eiermann, J. Mlynek, and V. Sandoghdar, Opt. Lett. **24**, 581 (1999).
[4] A. Rahmani, P. C. Chaumet, F. de Fornel, and C. Girard, Phys. Rev. A **56**, 3245 (1997).
[5] C. Henkel and V. Sandoghdar, Opt. Commun. **158**, 250 (1998).
[6] G. Parent, D. V. Labeke, and D. Barchiesi, J. Opt. Soc. Am. A **16**, 896 (1999).
[7] A. Rahmani, P. C. Chaumet, and F. de Fornel, Phys. Rev. A **63**, 023819 (2001).
[8] A. Madrazo and M. Nieto-Vesperinas, J. Opt. Soc. Am. A **13**, 785 (1996).
[9] C. Rockstuhl, M. G. Salt, and H. P. Herzig, J. Opt. Soc. Am. A **20**, 1969 (2003).
[10] P. A. Knipp and T. L. Reinecke, Phys. Rev. B **54**, 1880 (1996).
[11] M. Thomas, J.-J. Greffet, R. Carminati, and J. R. Arias-Gonzalez, Appl. Phys. Lett. **85**, 3863 (2004).
[12] L. Rogobete, H. Schniepp, V. Sandoghdar, and C. Henkel, Opt. Lett. **28**, 1736 (2003).
[13] G. S. Agarwal, Phys. Rev. A **12**, 1475 (1975).
[14] J. M. Wylie and J. E. Sipe, Phys. Rev. A **30**, 1185 (1984).
[15] M. S. Tomaš and Z. Lenac, Phys. Rev. A **56**, 4197 (1997).
[16] K. Joulain, R. Carminati, J.-P. Mulet, and J.-J. Greffet, Phys. Rev. B **68**, 245405 (2003).
[17] H. T. Dung, L. Knöll, and D.-G. Welsch, Phys. Rev. A **57**, 3931 (1998).
[18] S. Scheel, L. Knöll, and D.-G. Welsch, Phys. Rev. A **60**, 4094 (1999).
[19] A. Rahmani and G. W. Bryant, Phys. Rev. A **65**, 033817 (2002).
[20] V. V. Klimov and V. S. Letokhov, Chem. Phys. Lett. **301**, 441 (1999).
[21] M. S. Tomaš, Phys. Rev. A **63**, 053811 (2001).
[22] M. Nieto-Vesperinas, *Scattering and Diffraction in Physical Optics* (Wiley, New York, 1991).
[23] R. F. Harrington, *Field Computation by Moment Methods* (IEEE Press, Piscataway, 1993).

[24] C. Bohren and D. Huffman, *Absorption and Scattering of Light by Small Particles*, Wiley Science Paperback Series (Wiley, New York, 1998).
[25] P. B. Johnson and R. W. Christy, Phys. Rev. B **6**, 4370 (1972).
[26] J. D. Jackson, *Classical Electrodynamics*, 2nd ed. (Wiley, New York, 1975), Chap. 7.
[27] V. V. Klimov, M. Ducloy, and V. S. Letokhov, Quantum Electron. **31**, 569 (2001).
[28] A. F. Stevenson, J. Appl. Phys. **24**, 1134 (1953).
[29] M. Kreiter, M. Prummer, B. Hecht, and U. P. Wild, J. Chem. Phys. **117**, 9430 (2002).
[30] J.-Y. Courtois, J.-M. Courty, and J. C. Mertz, Phys. Rev. A **53**, 1862 (1996).
[31] W. L. Barnes, J. Mod. Opt. **45**, 661 (1998).
[32] L. Novotny, Appl. Phys. Lett. **69**, 3806 (1996).
[33] L. Novotny, Ph.D. thesis, ETH Zürich, 1996.
[34] R. J. Glauber and M. Lewenstein, Phys. Rev. A **43**, 467 (1991).
[35] G. Nienhuis and C. T. J. Alkemade, Physica B & C **81**, 181 (1976).
[36] V. V. Batygin and I. N. Toptygin, *Problems in Electrodynamics* (Academic Press, London, 1965), problem No. 200.
[37] J.-B. Thibaud, Ph.D. thesis, Ecole Centrale Paris, 2000.
[38] V. V. Klimov, M. Ducloy, and V. S. Letokhov, Eur. Phys. J. D **20**, 133 (2002).
[39] H. Ditlbacher, J. R. Krenn, B. Lamprecht, A. Leitner, and F. R. Aussenegg, Opt. Lett. **25**, 563 (2000).